JECS 1598c
0955-2219(95)00107-7
Journal of the European Ceramic Society **16** (1996) 43–53

0955-2219/96/$15.00

Temperature Stability of Samarium-Doped α-Sialon Ceramics

Zhijian Shen,[a] Thommy Ekström[b] & Mats Nygren[b]*

[a]Department of Materials Science and Engineering, Zhejiang University, Hangzhou 310027, P. R. China
[b]Department of Inorganic Chemistry, Arrhenius Laboratory, University of Stockholm, S-106 92 Stockholm, Sweden

(Received 31 January 1995; revised version received 2 June 1995; accepted 9 June 1995)

Abstract

Dense Sm-doped α-sialon ceramics along the tie line $Sm_xSi_{12-4.5x}Al_{4.5x}O_{1.5x}N_{16-1.5x}$ between Si_3N_4 and $Sm_2O_3{\cdot}9AlN$ were prepared by hot-pressing at 1800°C. The materials were subsequently heat-treated at different temperatures in the range 1300–1750°C for different times. The samples were either cooled by turning the furnace off, yielding a cooling rate (T_{col}) ≈ 50°C min^{-1} or quenched (T_{col} ≥ 400°C min^{-1}) by quickly moving the samples to a connected cooling chamber. It was found necessary to apply this quenching technique in order to reveal the true phase relations at high temperatures. It was found from phase analysis of quenched samples that the α-sialon phase is formed for 0·3< x <0·61, in equilibrium with a liquid phase. The α-sialon was only stable at temperatures above 1650°C, while at lower temperatures it transformed to the more stable β-sialon modification together with an Al-containing Sm melilite (M') phase. The z-value of β-sialon as well as the Al content of the M'-phase were found to correlate with the degree of α-sialon decomposition. This decomposition affects also the microstructure of the ceramics, i.e. small and almost equi-axed β-sialon grains form together with the M'-phase crystals located at the grain boundaries. The mechanical properties deteriorate: both hardness and fracture toughness of the materials decrease from 21 to 20 GPa and 4·5 to 2·5 MPa m$^{1/2}$ for unaged and aged samples, respectively.

1 Introduction

Sialon-based ceramics have gained attention in recent years, because it has become obvious that these materials in general combine less expensive preparation techniques with a possibility of controlling the mechanical properties by fairly simple means.[1–3] By altering the overall composition slightly, or by replacing the commonly used yttria sintering aid by other rare-earth element oxides, both hardness and fracture toughness can be changed in a controlled way. Recently, it has also been shown that the phase composition and the microstructure of α–β-sialon ceramics can be greatly affected by heat-treatment procedures when rare-earth oxides are used as sintering aids.[4] The α-sialon phase was observed to be less stable at lower temperatures and decomposed partly to rare-earth rich intergranular phases and β-sialon with a remarkably elongated crystal shape. It was pointed out by Mandal and co-workers that this might open another way of controlling the mechanical properties of the final sialon ceramics.[4]

The presence of α-sialon in the α–β-sialon ceramics contributes especially to the hardness, which is an important physical property in many applications where high abrasive wear resistance is crucial, e.g. in metal cutting tools.[1] The monophasic α-sialon ceramic is therefore an interesting material as the ultimate hardness for the sialon ceramics is achieved, but preparations must be made within restricted overall compositions.[2] The general formula for α-sialon can be expressed as $R_xSi_{12-(m+n)}Al_{m+n}O_nN_{16-n}$, where m(Si–N) are replaced by m(Al–N), and n(Si–N) by n(Al–O), and the valency discrepancy introduced by the former process is compensated by the R metal cation. The elements R which have been reported so far to stabilize the α-sialon modification are Li, Mg, Ca, Y, and the rare-earth metals except La, Ce, Pr, and Eu.[5,6] Although all the mentioned cations or combinations of these can stabilize the α-sialon structure, extensive studies have mainly been carried out in the yttrium-containing system.[7–11] In the latter system the α-sialon compositional field has a fairly small two-dimensional extension in the plane Si_3N_4– $Al_2O_3{\cdot}AlN$–$YN{\cdot}3AlN$.[2,7] Studies of the subsolidus phase relationships in Si_3N_4–AlN–rare-earth oxide systems at 1700°C show that the

*To whom correspondence should be addressed.

different rare-earth stabilized α-sialons have compositional fields quite similar to that of the yttrium-doped α-sialon. The only difference is that the solubility limits of the rare-earth element stabilized α-sialon widen slightly with decreasing size of the rare-earth cations.[6]

The most widely used preparation route for α-sialon ceramics is high-temperature liquid-phase sintering using α-Si_3N_4, AlN and appropriate metal oxides powders as starting materials. Many previous studies have been devoted to the reaction sequences occurring during the heating part of the sintering cycle, i.e. in the yttrium-doped[12] or in the other rare-earth metal-doped α-sialon systems.[13–15] These studies show that the formation of yttrium- and rare-earth metal-stabilized α-sialon have similar reaction sequences. At temperatures above the lowest eutectic, yttrium- or rare-earth rich intermediate oxide or oxynitride phases tend to form in small amounts, re-dissolving at higher temperatures, around 1500°C, when the formation of the α-sialon phase starts. The melilite phases, $R_2O_3{\cdot}Si_3N_4$, often containing aluminium in solid solution (M'-phases), thus occur frequently together with the α-sialon but dissolve at higher temperatures. Melilite is thus transiently formed during heating to the sintering temperature, and the amount of M'-phase is usually fairly large for the rare-earth metals Nd and Sm. The amount of M'-phase obtained passes through a maximum between 1500 and 1600°C. The decomposition of the M'-phase releases a large amount of the doping element, which facilities the precipitation of α-sialon and assists the final densification. The melting point of the melilite phase is therefore of importance, and Cheng and Thompson showed that the relatively low melting point of the Sm-doped M'-phase gave improved densification compared with Nd-doped ceramics, where the melilite phase had a considerably higher melting temperature.[15]

Very few studies have been concerned with changes in the phase assembly that might take place during the cooling part of the sintering cycle. After sintering the furnace is normally turned off and left to cool, and it is generally believed that only minor reactions, if any, take place during the cooling. Most post sintering studies have been directed towards the effects of prolonged heat treatments at temperatures substantially lower than the sintering temperature in order to crystallize the glassy grain-boundary phase in an attempt to obtain better high-temperature properties. However, it was surprisingly shown recently by Mandal and co-workers[4] and by Ekström and Shen[17] that the cooling rate applied from the sintering temperature to a great extent determines the microstructure of α-sialon containing ceramics. The α-sialon thus seems to be unstable at temperatures below 1600°C and decomposes to other phases, and new β-sialon crystals are formed. Recent independent work by Cheng and Thompson[15,16] on post heat treatment of Sm-doped α-sialon ceramics at 1500–1600°C confirmed these findings, and they observed a decrease of the α-sialon content accompanied by an increase of the M'-phase (as precipitate at the grain boundaries), and β-sialon was also formed in increasing amounts.

Our present work on silicon nitride based ceramics is devoted to studies on the relative stability of different rare-earth doped α-sialon phases in both pure α- and mixed α- and β-sialon systems. Some preliminary studies indicated that the stability of the α-sialon depends on the rare-earth element used.[17] The decomposition of α-sialon was also temperature-dependent and most easily seen in systems where larger cations like Nd and Sm were used, or when a residual liquid phase was present to aid the process. In these cases some post sintering reactions can take place even with 'normal' cooling rates (~40–50°C min^{-1}). In this article we will report a more detailed study of the phase stability of the samarium-doped α-sialon system. This is partly because it has been reported that the sinterability of samarium-doped sialon ceramics is excellent,[15] and additional knowledge of the thermal stability of these ceramics is therefore of importance. The effect on the mechanical properties is also of great interest. We have prepared a great number of samples along the Si_3N_4–$Sm_2O_3{\cdot}9AlN$ join line within the α-sialon plane mentioned above, and the α-sialon forming region and the thermal stability of the formed α-sialon along this line is assessed. The relation between the thermal stability of Sm-stabilized α-sialon and the formation of other Sm-rich phases like the M'-phase will be discussed, as well as the variation of the microstructure and the mechanical properties with the degree of decomposition of the α-sialon phase.

2 Experimental Procedure

The compositions selected for the present work were located on the join between Si_3N_4 and $Sm_2O_3{\cdot}9AlN$, with the overall compositions $Sm_x Si_{12-4.5x}Al_{4.5x}O_{1.5x}N_{16-1.5x}$ where x = 0·25, 0·35, 0·4, 0·6, 0·7, 0·8 and 1·0. Starting powders were Si_3N_4 (Ube, SN-E10), AlN (H.C. Starck-Berlin, grade A) and Sm_2O_3 (99·9%, Johnson Matthey Chemicals Ltd). The samarium oxide was calcined at 1000°C for 2 h before use, to remove any adsorbed water. When calculating the composi-

Table 1. Overall composition for samples of $Sm_xSi_{12-4.5x}Al_{4.5x}O_{1.5x}N_{16-1.5x}$ system

Sample no.	*Overall x-value*	*Amounts (wt%)*[a]		
		Sm_2O_3	Si_3N_4	*AlN*
ASM025	0·25	7·29	85·54	7·76
ASM035	0·35	9·95	80·03	10·59
ASM04	0·4	11·24	77·37	11·95
ASM06	0·6	16·10	67·32	17·11
ASM07	0·7	18·36	62·63	19·53
ASM08	0·8	20·53	58·14	21·82
ASM10	1·0	24·58	49·75	26·14

[a]The total amount of Sm_2O_3+Si_3N_4+AlN exceeds 100% in order to compensate for the excess oxygen content of Si_3N_4 and AlN.

tions of the samples, corrections were made for the small amounts of oxygen present in the Si_3N_4 and AlN raw materials. The analysed oxygen content of the silicon nitride powder corresponded to 2·74 wt% SiO_2 and of the aluminium nitride powder to 1·9 wt% Al_2O_3. The overall compositions (wt%) after correction are listed in Table 1.

The carefully weighed starting materials (50 g) were mixed/milled in water-free propanol for 24 h in a rotating plastic jar, using sialon media. Pellets of dried powders (about 5 g) were first compacted in a steel die, followed by hot-pressing (HP) in nitrogen for 2 h at 1800°C and 25 MPa in a graphite resistance furnace. The hot-pressed samples were then cooled at a rate (T_{col}) of ~50°C min^{-1} to 1000°C, i.e. much slower than the quenched samples prepared as described below, with $T_{col} \geq$ 400°C min^{-1}.

Selected specimens were subsequently heat-treated in different ways. Some samples were embedded in a mixture of Si_3N_4, AlN and BN packing powder in a carbon crucible and re-heated in nitrogen to 1750°C in a normal graphite sintering furnace. After heat treatment for 30 min at this temperature, some samples were quenched to room temperature by quickly moving them to a separate cooling chamber attached to the furnace. Other samples were quenched from 1750 to 1650 or to 1550°C and held at this temperature for another 24 h before quenching to room temperature. Samples quenched from 1750°C to room temperature were re-heated either to 1300 or 1450°C and held (embedded in the same powder bed as above) at these temperatures in nitrogen for up to 30 days in order to allow a study of the effects of prolonged heat treatments at lower temperatures on the phase content of the samples.

The densities of the sintered specimens were measured according to Archimedes principle. Before physical characterization, the specimens were ground and polished using standard techniques. Hardness (HV10) and indentation fracture toughness (K_{1c}) at room temperature were obtained with a Vickers diamond indenter with a 98 N (10 kg) load, and the fracture toughness was evaluated according to the method of Anstis *et al.*,[18] assuming a value of 300 GPa for Young's modulus.

Crystalline phases were characterized by their X-ray diffraction (XRD) patterns obtained in a Guinier–Hägg focusing camera with Si as internal standard. The X-ray films were evaluated with a computer-linked SCANPI system,[9] and the cell parameters were determined with use of the program PIRUM.[20] The z-value of the β-sialon phase, $Si_{6-z}Al_zO_zN_{8-z}$, was obtained from the mean values of z_a and z_c given by the following equations:[21]

$$a = 7{\cdot}603 + 0{\cdot}0297z \text{ Å}$$
$$c = 2{\cdot}907 + 0{\cdot}0255z \text{ Å} \quad (1)$$

The x-value of the melilite (M') solid solution $Sm_2Si_{3-x}Al_xO_{3+x}N_{4-x}$ was obtained using the equations given by Cheng and Thompson:[16]

$$a = 7{\cdot}690 + 0{\cdot}049x \text{ Å}$$
$$c = 4{\cdot}985 + 0{\cdot}037x \text{ Å} \quad (2)$$

In the quantitative estimation of the amounts of crystalline phases, the integrated intensities of the following reflections were used: (1 0 2) and (2 1 0) of the α-sialon, (1 0 1) and (2 1 0) of the β-sialon, and (2 1 1) of the Sm-melilite phase. The corrected relative weight fraction of each phase was then calculated from the expression:

$$W_k = (I_k/K_k)/\sum_{i=1}^{n}(I_i/K_i) \quad 1 \leq k \leq n \quad (3)$$

where W_k is the weight fraction of phase k, n is the number of crystalline phases present, and K_i is a constant for the intensity I_i of the selected reflection ($h\,k\,l$) of phases i. The K_i constants were calculated theoretically according to a procedure outlined in Ref. 22, and experimentally determined using calibration curves.

After application of a carbon coating, polished surfaces of hot-pressed and heat-treated samples were examined in a scanning electron microscope (Jeol JSM 820, equipped with a Link 10000 EDX analyser). The Si, Al and Sm contents were determined by energy dispersive X-ray (EDX) analysis, and the data given below are obtained from calibration curves and represent mean values of at least five point measurements.

3 Results and Discussion

The hot-pressed (1800°C) samples were found to be fully densified, as revealed by optical and

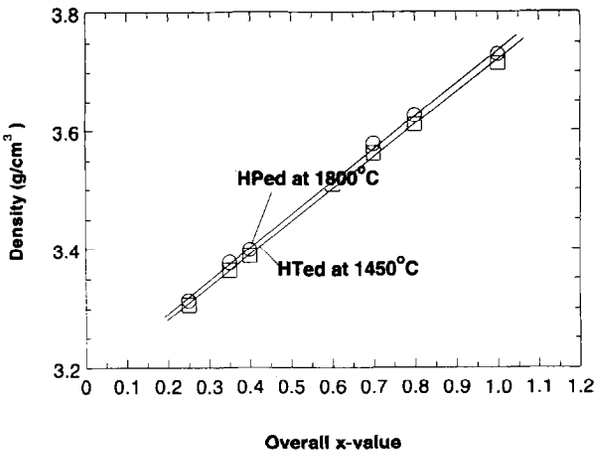

Fig. 1. Density as a function of the overall composition (x-value) in $Sm_xSi_{12-4.5x}Al_{4.5x}O_{1.5x}N_{16-1.5x}$ for samples hot-pressed at 1800°C (25 MPa, 2 h) as well as for samples subsequently heat-treated at 1450°C for 24 h.

scanning electron microscopy studies on polished cross-sections of sintered bodies. The observed density as a function of the overall x-value for α-sialon samples, both hot-pressed (HP) and post heat-treated (HT) at 1450°C for 24 h, are shown in Fig. 1. The density increases with increasing amount of Sm in both cases, as expected. The heat-treated samples have a slightly lower density than the hot-pressed samples, but no porosity was found in either type. Thus the difference in density may be assumed to reflect mainly the changes occurring when α-sialon is partly decomposed to form minor amounts of other phases, yielding a compact with a lower density, see below. It should also be mentioned that the samples re-heated at 1750°C, quenched to 1550–1650°C and heated for extended periods of time at these temperatures showed a slight weight loss which, however, never exceeded 2 wt%. This weight loss is probably due mainly to volatilization of SiO and should not significantly affect the microstructure and mechanical properties of the material (determined from the interior of the compacts).

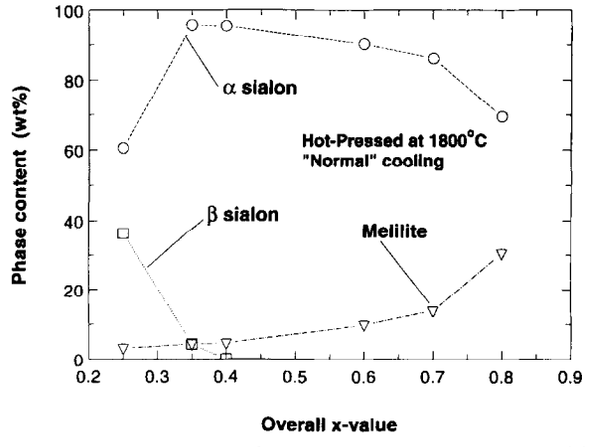

Fig. 2. Phase content as a function of the overall composition of $Sm_xSi_{12-4.5x}Al_{4.5x}O_{1.5x}N_{16-1.5x}$. The data refer to samples hot-pressed (1800°C) and normally cooled (~ 50°C min^{-1}).

3.1 On the α-sialon formation along the Si_3N_4–Sm_2O_3·9AlN line

Figure 2 shows the relation between the observed phase contents of hot-pressed samples, cooled at a rate of ~ 50°C min^{-1}, and the overall composition of the α-sialon. In the range $0{\cdot}25 \leq x \leq 0{\cdot}35$ the materials consisted mainly of two phases, namely α- and β-sialon, but a minor amount of the melilite phase is also found. In the range $0{\cdot}40 \leq x \leq 0{\cdot}60$ the major phase was α-sialon, but all materials also contained some melilite phase, increasing in amount with increasing x-value. For higher x-values the amount of α-sialon decreased significantly, and besides melilite small amounts of Si–Al–O–N polytypoid phases were identified.

Hot-pressed and furnace cooled samples always contained some other crystalline phase besides α-sialon. These results show similarities with previous studies on Y-doped α-sialon.[11,12] The phase content of these samples, which were re-heated to 1750°C and held this temperature for 0·5 h before being quenched ($T_{col} \geq 400$°C min^{-1}) to room temperature, exhibited a different phase composition. In the range $0{\cdot}25 \leq x \leq 0{\cdot}35$ a two-phase α–β sialon mixture was found, but no crystalline grain-boundary phase was detected. Monophasic α-sialon compacts were obtained in the compositional range $0{\cdot}4 \leq x \leq 0{\cdot}8$, as demonstrated in Fig. 3. It should be stressed, however, that the apparently monophasic α-sialon samples contained some amorphous glassy phase (as will be shown below) and that the homogeneity range indicated in this figure does not represent the true solid solution range. The difference in the phase content of these compacts (see Figs 2 and 3) demonstrates that post heat treatment and cooling rate have a significant influence on amount and type of phases formed.

To further enhance the decomposition of the α-sialon phase, the HP compositions were heat-treated at 1450°C for 24 h. In this case even more melilite was obtained in all samples, accompanied

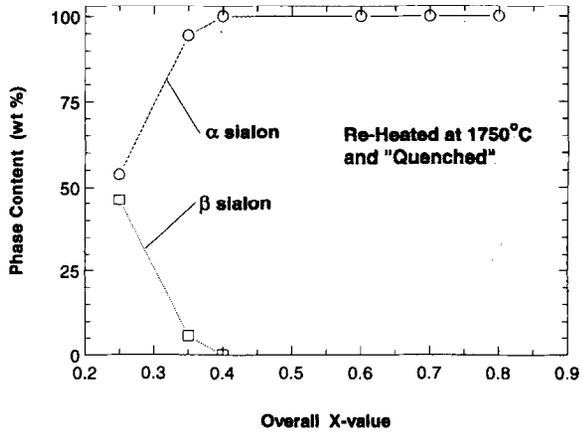

Fig. 3. Phase content as a function of the overall composition for samples quenched from 1750°C.

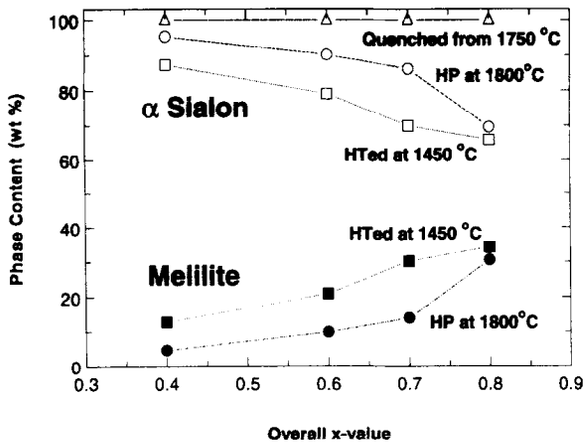

Fig. 4. Comparison of the phase composition for samples prepared in different ways, see text.

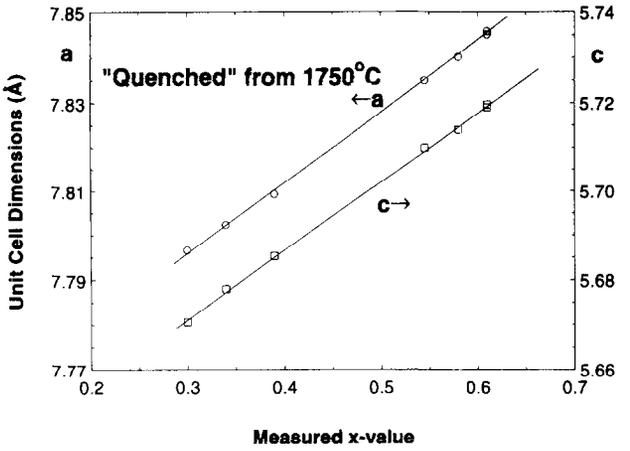

Fig. 6. Unit cell dimensions of α-sialon versus EDX-measured x-value for samples quenched from 1750°C, see text.

by a decrease of the α-sialon content as illustrated in Fig. 4. The formation of larger amounts of melilite at a holding time of 24 h at 1450°C should not be surprising. The very rapid initial formation of melilite in HP samples cooled at a rate of 50°C min^{-1} is somewhat more surprising, however, as the temperature range of M'- phase stability is traversed within 8 min. It has, however, previously been observed that melilite can be formed rapidly in these types of system.[17]

The samples quenched from 1750°C seem to be the ones which yield the most reliable picture of the conditions at high temperature. To accurately assess the extension of the α-sialon solid solution range along the investigated compositional line, it is also important to remember that the X-ray amorphous glassy phase might hold a considerable amount of the added samarium. The variation in unit cell dimensions of α-sialon in quenched samples as a function of the amount of added samarium (overall x-value) and the x-value measured by careful EDX analysis measurements of the α-sialon grains will give different results, as illustrated in Figs 5 and 6, respectively.

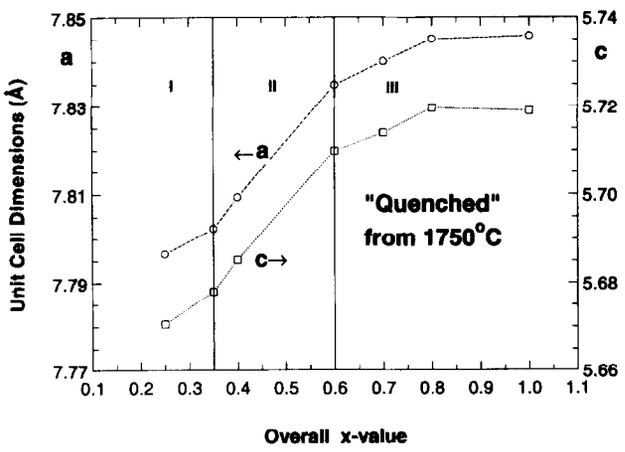

Fig. 5. Unit cell dimensions of α-sialon versus overall composition in $Sm_xSi_{12-4.5x}Al_{4.5x}O_{1.5x}N_{16-1.5x}$, for samples quenched from 1750°C.

The results shown in Fig. 5 are difficult to interpret (see below), and yet the extent of the solution range of α-sialons has been determined from similar diagrams in the past. The α-sialon lattice expands in both the a and c dimensions with increase of overall x-value, more or less over the whole investigated compositional range, but the steepest slope is obtained in range II. In ranges I and III, the α-sialon phase co-exists with β-sialon and polytypoid phases, respectively, suggesting that area II might represent a solid solution range. However, the shifts in lattice parameters plotted in Fig. 6 against measured x-values (including also data from α-sialon grains in the multi-phase areas I and III) show that the true solid solution range is most probably $0{\cdot}30 \leq x \leq 0{\cdot}61$ at 1750°C. The shift in unit cell dimensions of α-sialon as a function of the measured x-value can be expressed by the following relationships:

$$a = 7{\cdot}75 + 0{\cdot}158x \text{ Å}$$
$$c = 5{\cdot}62 + 0{\cdot}154x \text{ Å} \quad (4)$$

According to the formula $Sm_xSi_{12-4.5x}Al_{4.5x}O_{1.5x}N_{16-1.5x}$, the Si/Al atomic ratio of pure α-sialon on the Si_3N_4–Sm_2O_3·9AlN line can be expressed as

$$Si/Al = 2{\cdot}667x^{-1} - 1 \quad (5)$$

and is drawn as a solid line in Fig. 7, where the measured Si/Al atomic ratios of the α-sialon phase in the samples quenched from 1750°C are also plotted versus the measured x-value. It can be seen that the calculated and observed Si/Al ratios in the single-phase α-sialon range are in good agreement with each other. One sample at a low x-value has a somewhat lower observed Si/Al ratio, and one reason might be that this material is in a two-phase α–β-sialon area. The α-sialon composition in equilibrium with β-sialon might have slipped somewhat from the investigated compositional line and along the edge of the

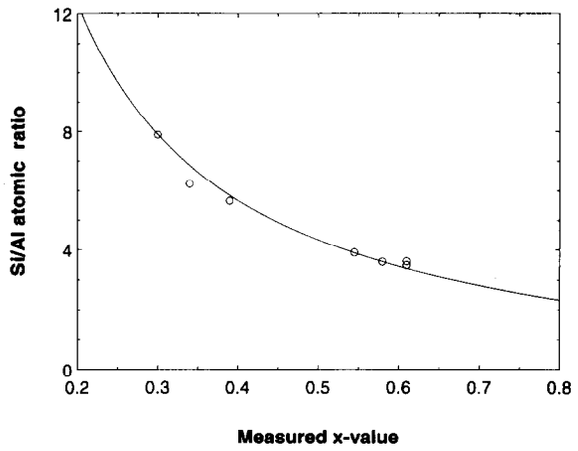

Fig. 7. Si/Al atomic ratio in α-sialon versus EDX-measured x-value for samples quenched from 1750°C, the solid line is obtained according to Eqn (5).

two-phase α-sialon region towards a lower Si/Al ratio. In any case, Fig. 7 shows that the composition of obtained α-sialon phase is close to the Si_3N_4– Sm_2O_3·9AlN line.

Using the relations between the lattice parameters and composition given in Eqn (4), the extension of the α-sialon forming region can be estimated for samples hot-pressed at 1800°C and for those post heat-treated at 1450°C for 24 h. The HP samples were found to have the same homogeneity range as those quenched from 1750°C, i.e. $0{\cdot}30 \leq x \leq 0{\cdot}61$, while the ones heat-treated at 1450°C had a slightly narrower range, $0{\cdot}30 \leq x \leq 0{\cdot}55$, indicating that the high x-value limit is temperature-dependent.

Scanning electron micrographs of typical samples quenched from 1750°C are shown in Fig. 8 (recorded in back-scattered electron mode). The α-sialon phase appears with grey contrast in the micrographs and the samarium-rich amorphous intergranular phase with a white contrast, while the β-sialon grains in the samples appear black and have the typical elongated shape of hexagonal rods.

The micrograph of a sample in the mixed α–β-sialon range (with an overall composition of $x = 0{\cdot}25$) revealed the presence of very elongated β-sialon grains (with a z-value 0·39) and equi-axed α-sialon grains having a grain size distribution ranging from 0·2 to 4 μm (see Fig. 8(a)). For compositions close to the α–β boundary ($x = 0{\cdot}35$) some β-sialon still existed in the α-sialon structure, as seen in Fig. 8(b). The microstructure of the samples in the single-phase α-sialon range consisted predominantly of α-sialon grains, which were surrounded by some residual amorphous intergranual phase, and the content of amorphous phase increased with the increasing overall x-value. For even higher x-values ($x \geq 0{\cdot}80$) the microstructure contained more glassy phase and small, dark, plate-like polytypoid crystals.

A new phase with bright SEM appearance was formed in the samples with $x \geq 0{\cdot}8$. This new phase occurred as white squares (indicating it to be Sm-rich) in the SEM micrographs at low magnification, see Fig. 8(e). According to the EDX analysis these white areas had a metal composition of Si (65·4 at%), Al (22·7 at%) and Sm (12·6 at%). However, at high magnification one can easily see that some elongated grains are present in the matrix of this phase (see Fig. 8(f)), and the EDX analysis suggested them to be α-sialon grains. Some of these α-sialon crystals have aspect ratios of up to 10. Although elongated α-sialon crystals have sometimes been noted in the past, aspect ratios of this magnitude have never been seen. It thus seems likely that this Sm-rich matrix promotes growth of elongated α-sialon grains.

3.2 On the formation of melilite solid solutions during cooling part of the sintering cycle

Two HP samples, ASM04 and ASM06, were quenched (after being heat-treated for 24 h) from different temperatures in the range $1300 \leq T \leq 1650$°C in order to find the optimal precipitation temperature and determine the thermal stability range of the samarium-based M'-phase. The obtained data are summarized in Fig. 9. It should be noted that some M'-phase was present in the HP compacts used as starting material in this study (see Fig. 4) and that the same amount is found in samples heat-treated at 1300°C. This low temperature thus does not seem to cause any changes in the phase composition of the materials, which might be due to the fact that no liquid phase is present at this temperature. At higher heat-treatment temperatures, reaction took place however, and these temperatures are well above the eutectic liquid formation temperature. In the ASM04 sample, the maximum amount of M'-phase seems to have formed at 1450°C, and some M'-phase was still present in the sample heated at 1550°C but even less than in starting material. In the case of the ASM06 sample, the maximum amount of M'-phase also occurred in those heat-treated at 1450°C, and M' was still present after heat treatment at 1650°C.

The formation of the M'-phase at 1450°C was accompanied by a decrease of the α-sialon content as well as by a change of the unit cell dimensions of α-sialon, see Figs 9 and 10. Thus the M' formation is not solely the result of devitrification of the residual grain-boundary liquid phase but also due to the reaction:

$$\alpha_1 + \text{liquid} \rightarrow \alpha_2 + \text{M}' \qquad (6)$$

where α_2 is an α-sialon with a lower x-value than α_1. This process is similar to the one suggested by

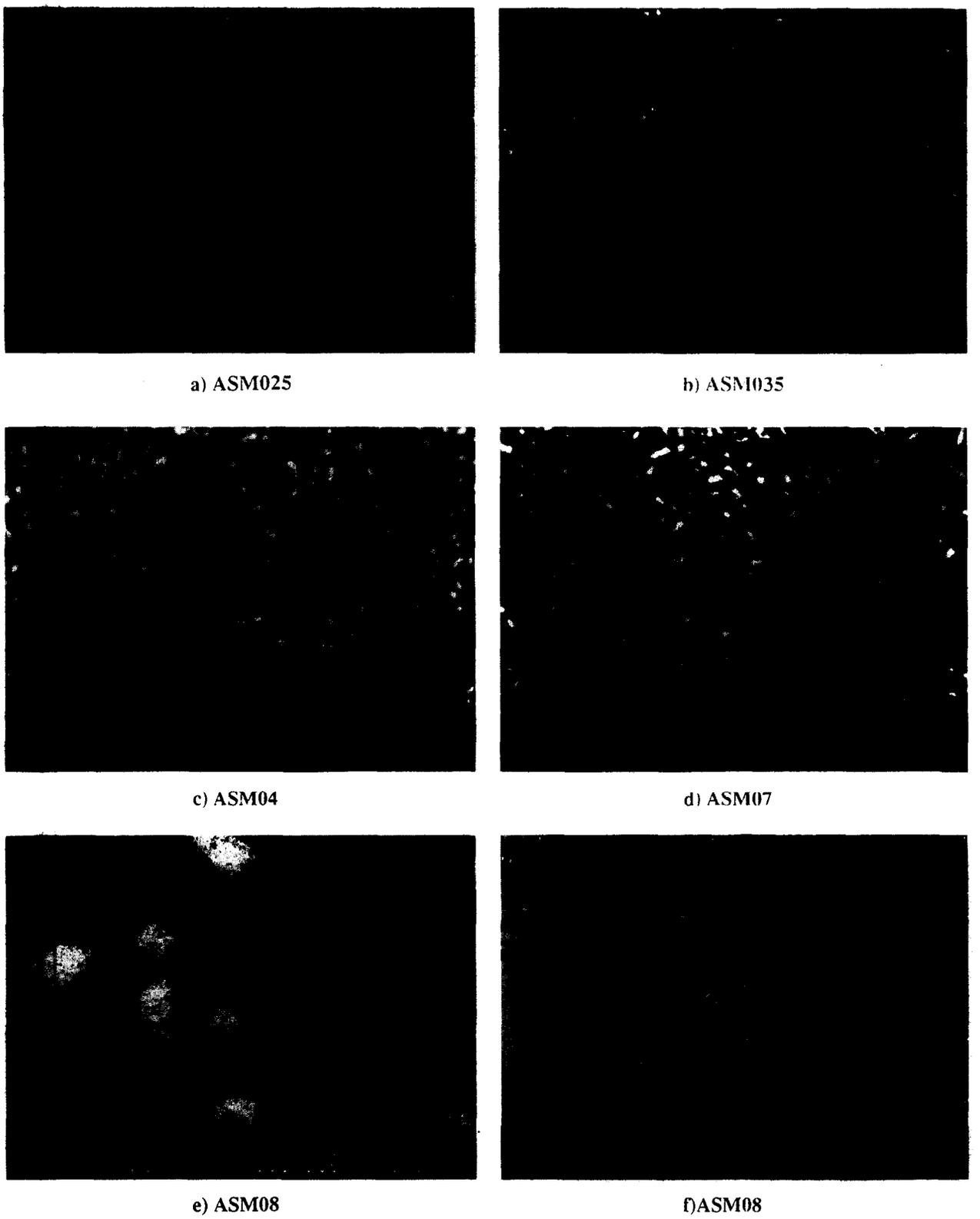

Fig. 8. Back-scattered SEM micrographs for samples quenched from 1750°C: (a) ASM025; (b) ASM035; (c) ASM04; (d) ASM07; (e) and (f) ASM08.

Cheng and Thompson[16] and is said to be valid for both Sm-based α- and α–β-sialon ceramics:

$$\alpha + \text{liquid} \rightarrow \beta + \text{M}' \qquad (7)$$

In this case the M'-phase formation is thus accompanied by $\alpha \rightarrow \beta$ transformation. Both possibilities seem to be reasonable, but might occur under different conditions. The key point is, however, that in both cases the liquid takes an active part in the reaction.

Heat treatment of the hot-pressed α-sialon compacts at 1650°C, which is close to the decomposition temperature of the M'-phase, generally leads to a grain coarsening of α-sialon (see Fig. 11). In the HP material, most of the initially present M'-phase dissolved, implying that the overall α-sialon grain composition tends to move towards

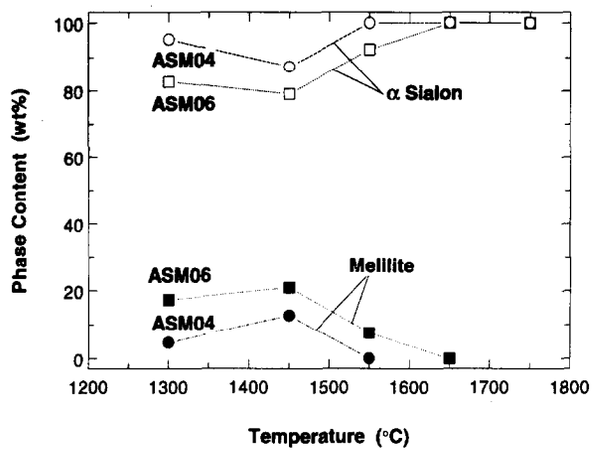

Fig. 9. Phases present in ASM04 and ASM06 samples after heat treatment at different temperatures for 24 h.

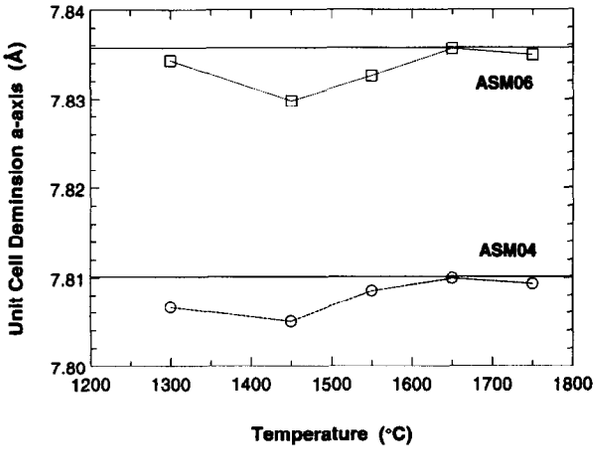

Fig. 10. Unit cell dimensions of α-sialon in ASM04 and ASM06 samples after heat treatment at different temperatures for 24 h.

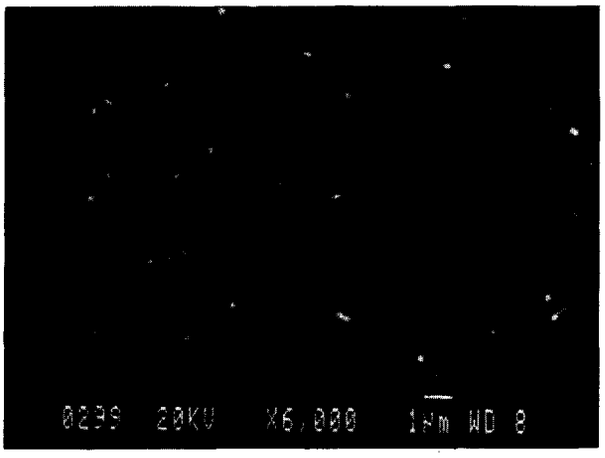

Fig. 11. Back-scattered SEM micrographs for ASM04 sample quenched from 1650°C after heat treatment for 24 h.

that found in samples quenched from 1750°C (see the unit cell dimensions in Fig. 10). The unit cell of α-sialon is, however, slightly larger at 1650°C than at 1750°C, possibly because the Sm released when the M'-phase dissolves is mainly taken up by the α-sialon and not to the same extent by the liquid. This means that true equilibrium between the liquid phase, the M'-phase and the α-sialon phase is not reached.

Previous work on the reaction sequence occurring during heating of the samarium-doped α-sialon system has shown that the M'-phase is transiently formed, melting at about 1700°C.[13–15] The present results confirm that samples heat-treated at 1750°C and quenched do not contain any M'-phase. However, samples exposed to a 'normal' cooling rate of 50°C min^{-1} do contain some M'-phase, which shows that the M'-phase forms rapidly upon cooling. This cooling rate is similar to that used by Cheng and Thompson when they prepared two Sm-doped α-sialons with $x \approx 0{\cdot}4$[15,16] In all essential parts their phase analysis can also be interpreted on the basis that the main part of the M'-phase is formed during the cooling process.

3.3 Decomposition of samarium-doped α-sialon

From the results presented above we know that the initial formation of melilite M'-phase is rapid, but not what is going to happen during prolonged heat treatment. A pure α-sialon (sample ASM04) was therefore heat-treated at 1450°C from 1 to 30 days in a protective nitrogen atmosphere. The result of the phase analysis is summarized in Fig. 12. This study shows that α-sialon transforms to M'-phase and β-sialon upon prolonged heat treatment but that during the first 24 h of heat treatment the amount of M'-phase is dramatically increased (accompanied by a decrease of α-sialon content) without β-sialon formation. The initial reaction can therefore be expressed by Eqn (6) given above. When the M'-phase is formed, the composition of the α-sialon grains changes as seen in Fig. 13.

Prolonged heat treatment yields more M'-phase, accompanied by formation of β-sialon grains. During this process the composition of the residual α-sialon remains constant (see Fig. 13), indicating a different reaction pathway. The mechanism suggested by Cheng and Thompson[16] for Sm-doped α-sialon ceramics (Eqn(7)) might be possible, but

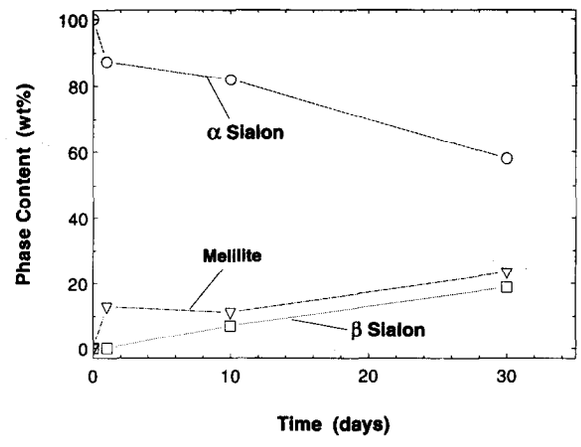

Fig. 12. Phases present in ASM04 samples after heat treatment at 1450°C for 1–30 days.

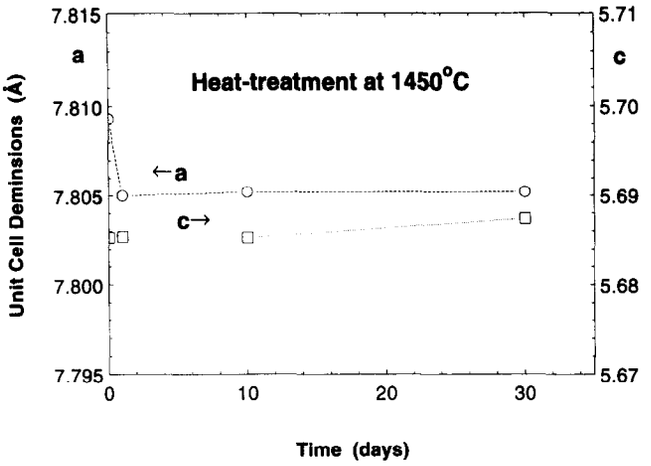

Fig. 13. Unit cell dimensions of α-sialon in ASM04 samples after heat treatment at 1450°C for 1–30 days.

our data do not exclude a reaction pathway such as:

$$\alpha \rightarrow \beta + \mathrm{M}' \qquad (8)$$

The changes in microstructure were followed by recording back-scattered SEM micrographs of ASM04 samples after different times of heat treatment at 1450°C, and the results are illustrated in Fig. 14. Some systematic structure differences are noticed, firstly by comparison with the micrograph of the same sample quenched from 1750°C (Fig. 8(c)). As shown above (Fig. 8(c)), the microstructures of quenched samples (from 1750°C) predominantly consisted of α-sialon grains surrounded by some residual grain-boundary glass phase. Heat treatment at 1450°C for 1 day resulted in inhomogeneous precipitation of the M'-phase. Thus, in accordance with Cheng and Thompson,[16] large areas containing no or very small amounts of residual glassy grain-boundary phase were found, see Fig. 14.

The XRD and EDX studies confirmed that the melilite formed after 1 day of heat treatment had the composition $Sm_2Si_{3-x}Al_xO_{3+x}N_{4-x}$ with $x \approx 0{\cdot}7$. The compositions of the M'-phase and β-sialon phase changed with further heat treatment. Thus the z-value of the formed β-sialon decreased from $z = 0{\cdot}33$ (10 days) to 0·25 (30 days), and a slight increase of the x-value of M'-phase occurred from $x = 0{\cdot}28$ (10 days) to 0·66 (30 days). This indicates that the α-sialon decomposition is a diffusion-controlled process, and the α-sialon content, the amount and composition of β-sialon and of M'-phase are correlated. In summary, the results show that in the temperature region $1300 < T \leq 1650$°C the α-sialon formed at higher temperatures decomposes into the more stable M'- and β-sialon phases.

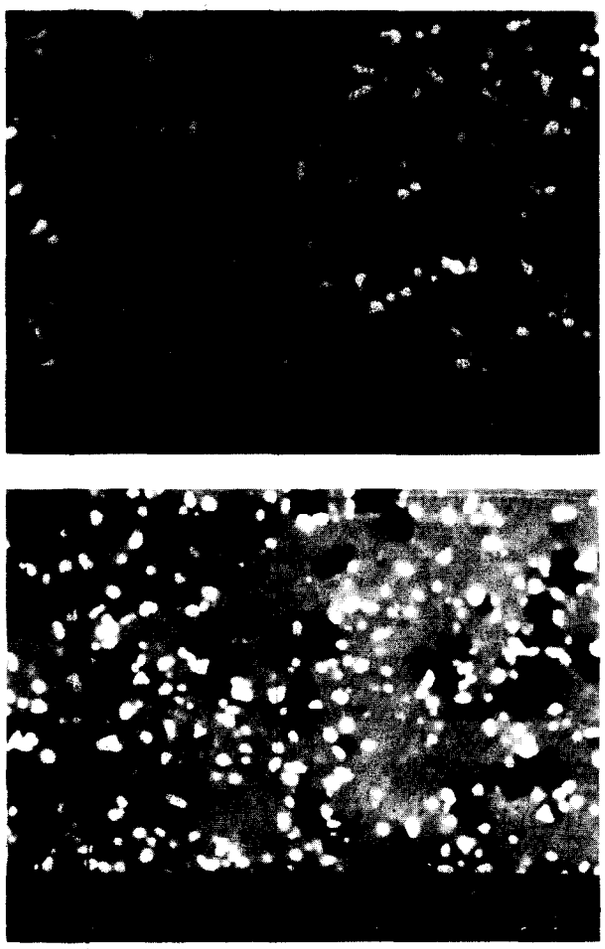

Fig. 14. Back-scattered SEM micrographs for samples heat-treated at 1450°C for (a) 10 and (b) 30 days.

3.4 Mechanical properties

The Vickers hardness (HV10) and the indentation fracture toughness (K_{1c}) were measured for hot-pressed and heat-treated samples at room temperature. The results for hot-pressed samples are shown in Fig. 15. The general trend is that the mixed α–β-sialon materials in range I have higher toughness but lower hardness, whereas the α-sialon in range II is very hard but brittle. Materials in the range III, which contain more glass and some sialon polytypoids, are even more brittle.

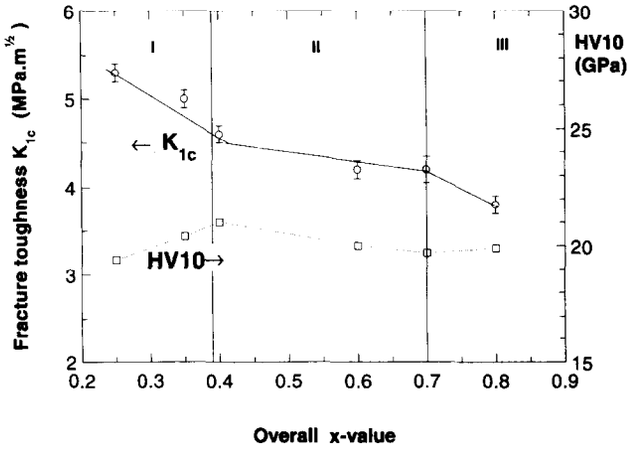

Fig. 15. Vickers hardness HV10 and indentation toughness K_{1c} for samples hot-pressed at 1800°C.

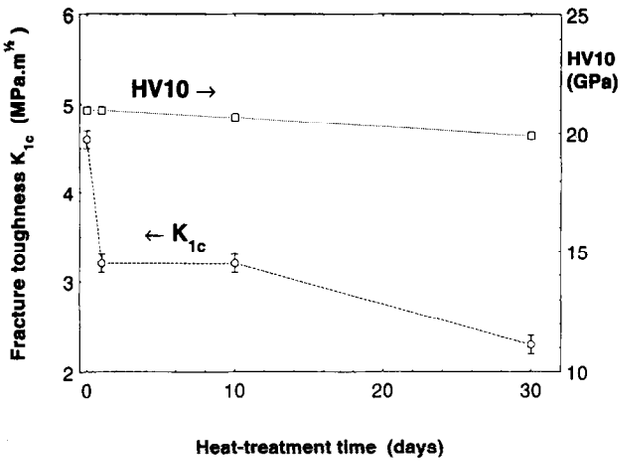

Fig. 16. Vickers hardness HV10 and indentation toughness K_{1c} for ASM04 samples heat-treated at 1450°C, as functions of the time of heat treatment.

The hardness of mixed α–β-sialons in range I increases with increasing α-sialon content; however, the toughness changed in the opposite way as previously found for α–β-sialons in other systems.[1,3] The highest hardness values were obtained for materials in range II ($0{\cdot}35<x<0{\cdot}7$), in agreement with the fact that these materials have the highest α contents. The drop in hardness that occurs in range III can be explained by the decrease of the α-sialon content and the presence of increasing amounts of both intergranular phases and sialon polytypoids.

The Vickers hardness (HV10) and indentation fracture toughness (K_{1c}) for the samples (ASM04) heat-treated at 1450°C are given in Fig. 16. Both HV10 and K_{1c} decrease with increasing time of heat treatment. This can be understood in terms of the shifts in phase composition discussed above.

4 Conclusions

(1) α-Sialon is a stable phase and can co-exist with a liquid phase at temperatures exceeding 1550–1650°C (depending on the α composition) in the Sm-doped α-sialon system. The homogeneity range for $Sm_xSi_{12-4{\cdot}5x}Al_{4{\cdot}5x}O_{1{\cdot}5x}N_{16-1{\cdot}5x}$ was found to be $0{\cdot}30< x <0{\cdot}61$.

(2) α-Sialon grains formed at high temperatures decompose into β-sialon and an Al-containing Sm-melilite (M') phase when re-heated at temperatures below 1550–1650°C. This reaction is diffusion controlled. The amounts and compositions of the α-sialon, β-sialon and melilite M'-phases are strongly correlated.

(3) The M'-phase formation temperature depends on the overall composition of the α-sialon samples, and the M'-phase tends to form at a slightly higher temperature in the samples with higher Sm content. Most M'-phase is formed at temperatures just above the eutectic.

(4) The formation of the M'-phase by decomposition of α-sialon can proceed by two different mechanisms. Initially, M'-phase precipitation occurs as expressed in Eqn (6), yielding an α-sialon with lower Sm content. After devitrification of the residual grain-boundary liquid phase, the decomposition of α-sialon takes place as expressed in Eqn (8).

(5) When α-sialon decomposes, small and almost equi-axed β-sialon grains form together with a very fine-grained precipitate of the M'-phase, which leads to a decrease of both hardness and fracture toughness of the materials.

Acknowledgements

This study has been supported by the Swedish Research Council for Engineering Sciences. Zhijian Shen thanks the Swedish Institute for a scholarship during the period when the work was carried out.

References

1. Ekström, T., Effect of composition, phase content and microstructure on the performance of yttrium Si–Al–O–N ceramics. *Mater. Sci. Eng.*, **A109** (1989) 341–9.
2. Ekström, T. & Nygren, M., SiAlON ceramics. *J. Am. Ceram. Soc.*, **75** (1992) 259–76.
3. Ekström, T., Sialon ceramics sintered with yttria and rare earth oxides. *Mater. Res. Soc. Symp. Proc.*, **287** (1992) 121–32.
4. Mandal, H., Thompson, D. P. & Ekström, T., Reversible α–β-sialon transformation in heat-treated sialon ceramics. *J. Eur. Ceram. Soc.*, **12** (1993) 421–9.
5. Hampshire, S., Park, H. K., Thompson, D. P. & Jack, K. H., α-Sialon ceramics. *Nature*, London, **274** (1987) 88–82.
6. Huang, Z. K., Tien, T. Y. & Yen, T. S., Subsolidus phase relationships in Si_4N_4–AlN–rare earth oxide systems. *J. Am. Ceram. Soc.*, **69** (1986) C-241–2.
7. Sun, W. Y., Tien, T. Y. & Yen, T. S., Solubility limits of α-sialon solid solutions in the system Si, Al, Y/N,O. *J. Am. Ceram. Soc.*, **74** (1991) 2547–50.
8. Slasor, S. & Thompson, D. P., Preparation and characterisation of yttrium α-sialons. In *Non-oxide Technical and Engineering Ceramics*, ed. S. Hampshire, Elsevier, Amsterdam, Netherlands, 1985, pp. 223–9.
9. Ishizawa, K., Ayuzawa, N., Shiranita, A., Taki, M., Ushida, N. & Mitomo, M., Properties of α-sialon ceramics. *Yogyo Kyokaishi*, **94** (1986) 183–5.
10. Mitomo, M., Izumi, F., Babdo, Y. & Sekikawa, Y., Characterisation of α-sialon ceramics. In *Proc. Int. Symp. Ceram. Components Engine*, (1983) 377–86.
11. Bartek, A., Ekström, T., Herbertsson, H., & Johnsson, T., Yttrium α–β-sialon ceramics by hot isostatic pressing and post-hot isostatic pressing. *J. Am. Ceram. Soc*, **75**(2) (1992) 432–9.
12. Cao, G. Z., & Metselaar, R., α-SiALON ceramics: a review. *Chem. Mater.*, **3** (1991) 242–52.
13. Hampshire, S., Reilly, K. P. J. O., Leigh, L. & Redington, M., Formation of α–β SIALON with neodymium and samarium modifying cations. In *High Tech Ceramics*, ed. P. Vincenzini, Elsevier Publishers BV, Amsterdam, Netherlands, 1983, pp.933–40.

14. Wang, P. L., Sun, W. Y. & Yen, T. S., Sintering and formation behaviour of R–α-sialon (R=Nd, Sm, Gd, Dy, Er and Yb). *Eur. J. Solid State Inorg. Chem.*, **t.31**, (93) (1994) 104.
15. Cheng, Y. B. & Thompson, D. P., Preparation and grain boundary devitrification of samarium α-sialon ceramics. *J. Eur. Ceram. Soc.*, **14** (1994) 13–21.
16. Cheng, Y. B. & Thompson, D. P., Aluminium-containing nitrogen melilite phase. *J. Am. Ceram. Soc.*, **77** (1994) 143–8.
17. Ekström, T. & Shen, Z. J., Temperature stability of rare earth doped α-sialon Ceramics. In *5th Int. Symp. on Ceramic Materials and Components for Engines*, eds D. S. Yan, X. R. Fu & S. X. Shi, World Scientific, Singapore, 1995, pp. 206–10.
18. Anstis, G. R., Chantikul, P., Lawn, B. R. & Marshall, D. P., A critical evaluation of indentation techniques for measuring fracture toughness: I. direct crack measurements. *J. Am. Ceram. Soc.*, **64** (1981) 533.
19. Johansson, K.-E., Palm, T. & Werner, P.-E., An automatic microdensitometer for X-ray powder diffraction photographs. *J. Phys.*, **E13** (1980) 1289–91.
20. Werner, P.-E., A Fortran program for least-squares refinement of crystal structure cell dimension, *Arkiv för Kemi*, **31**(43) (1969) 513.
21. Ekström, T., Käll, P.-O., Nygren, M. & Olsson, P.-O., Dense single-phase β-sialon ceramics by glass-encapsulated hot isostatic pressing. *J. Mater. Sci.*, **24** (1989) 1853–61.
22. Käll, P.-O., Quantitative phase analysis of Si_3N_4-based materials. *Chem. Scripta*, **28** (1988) 439–46.